Photochemistry and Photobiology, 2004, 80: 7–14

Structural Heterogeneity of Cryotrapped Intermediates in the Bacterial Blue Light Photoreceptor, Photoactive Yellow Protein¶

Spencer Anderson,*[1,2] Vukica Šrajer[1,2] and Keith Moffat[1,2,3]

[1]Department of Biochemistry and Molecular Biology, University of Chicago, Chicago, IL
[2]Consortium for Advanced Radiation Sources, University of Chicago, Chicago, IL
[3]Institute for Biophysical Dynamics, University of Chicago, Chicago, IL

Received 15 March 2004; accepted 19 May 2004

ABSTRACT

We investigate by X-ray crystallographic techniques the cryotrapped states that accumulate on controlled illumination of the blue light photoreceptor, photoactive yellow protein (PYP), at 110 K in both the wild-type species and its E46Q mutant. These states are related to those that occur during the chromophore isomerization process in the PYP photocycle at room temperature. The structures present in such states were determined at high resolution, 0.95–1.05Å. In both wild type and mutant PYP, the cryotrapped state is not composed of a single, quasitransition state structure but rather of a heterogeneous mixture of three species in addition to the ground state structure. We identify and refine these three photoactivated species under the assumption that the structural changes are limited to simple isomerization events of the chromophore that otherwise retains chemical bonding similar to that in the ground state. The refined chromophore models are essentially identical in the wild type and the E46Q mutant, which implies that the early stages of their photocycle mechanisms are the same.

INTRODUCTION

Photoactive yellow protein (PYP) is a bacterial blue-light photoreceptor (1) that transduces the absorbed energy from a photon into a structural signal through progression through a fully reversible photocycle (2–4). The earliest intermediates in the PYP photocycle at room temperature form on an extremely fast timescale, from picoseconds to nanoseconds, and are therefore very difficult to detect structurally (5). The lifetimes of species related to these intermediates can be extended by forming a photostationary state under controlled, continuous illumination at cryogenic temperatures (6,7). The direct biological relevance of these low-temperature species can be questioned because their absorption maxima differ from those of the intermediate species formed at room temperature. However, recent spectroscopic (8) and structural (9) evidence suggests that certain low-temperature intermediates resemble those in the initial stages of the room temperature photocycle. Hence, low-temperature studies enable these initial stages to be probed (see Discussion).

A previous cryotrapping experiment on wild-type PYP at 149 K revealed that structural changes produced by illumination of the *trans* ground state are limited to the coumaric acid chromophore and its binding pocket (10). The most significant structural change occurred in the chromophore tail; the chromophore phenolic ring was only slightly displaced, and the hydrogen bond network between the surrounding protein and its phenolate oxygen was maintained. The photoactivated chromophore was refined in a single *cis* conformation with extremely strained bond angles. This unusual geometry led to the conclusion that much of the energy derived from absorption of the photon is captured in a structurally unstable chromophore (10) and to speculation that this *cis* conformation is similar to a transition state (11).

We are interested in the relationship between the photoactivated intermediates found in the cryotrapped state and the early, very short-lived intermediates in the room temperature photocycle. We investigate and compare the structural changes taking place in cryotrapped states at 110 K in both wild-type PYP and its isosteric E46Q mutant, a mutant with a quantitatively altered photocycle at room temperature (12,13).

MATERIALS AND METHODS

Data collection and processing. All crystals were prepared and X-ray diffraction data collected at 110 K as described (14). The cryotrapping experiments were performed under conditions intended to be closely similar to the previous experiment on wild-type PYP (10). Data collection protocols were identical for wild-type PYP and the E46Q mutant, and crystals of similar dimensions, 200 × 200 × 600 μm, were chosen. To minimize systematic errors arising from crystal-to-crystal variation, the same crystal was used to collect diffraction data for both the ground (dark) state and the cryotrapped state. Ground state data were collected for a 1 h period in a darkened hutch. The same crystal was then illuminated with filtered light from a Xe lamp at 480 nm (10 nm bandpass and 5 mW/mm^2) for 1 h with constant rotation to populate the cryotrapped state. Illumination was continued for a further hour during X-ray data collection on this state. DENZO and SCALEPACK (15) were used for indexing, integration, scaling and merging of monochromatic oscillation data. The ground state structures of both wild type and E46Q were refined as described (14).

Difference refinement. The cryotrapped state was refined using difference refinement relative to the ground state (16). That is, ($Fc^{cryotrap} - Fc^{dark}$) was refined against ($Fo^{cryotrap} - Fo^{dark}$). Difference refinement is especially suited to this refinement situation because both the dark and cryotrapped data were collected on the same crystal, and the structural differences between these states are spatially localized and small in magnitude. Indeed, the difference R between the cryotrapped and the dark data is extremely

¶Posted on the website on 28 May 2004

*To whom correspondence should be addressed: CARS, The University of Chicago, Argonne National Laboratory, Building 434-B, 9700 South Cass Avenue, Argonne, Illinois 60439. Fax: 630-252-0443; e-mail: smander@midway.uchicago.edu

Abbreviation: PYP, photoactive yellow protein.

Table 1. Crystallographic data and refinement statistics. All data were collected at 110 K*

	WT ground†	E46Q ground†	WT cryotrap	E46Q cryotrap
Resolution (Å)	1.00	0.95	1.05	0.95
$a = b$, c (Å)	66.21, 40.51	66.19, 40.50	66.25, 40.55	66.21, 40.52
Total observations	860 006	855 706	775 420	831 639
Unique reflections	54 493	63 595	47 321	63 522
Redundancy	15.8	13.5	16.4	13.1
Resolution range (Å) (last shell)	100–1.00 (1.04–1.00)	100–0.95 (0.98–0.95)	100–1.05 (1.09–1.05)	100–0.95 (0.98–0.95)
Completeness (%)‡	98.6 (95.4)	93.5 (78.5)	99.1 (96.7)	90.9 (60.0)
I/σ(I)‡	30.8 (7.2)	26.5 (4.4)	28.5 (8.9)	17.0 (3.8)
R_{merge}†§	5.7 (56.8)	4.6 (25.4)	6.5 (58.1)	6.1 (55.7)
R_{cryst}	13.39‖	14.37‖	5.83¶	6.91¶
R_{free}#	16.14	16.11	6.43	7.61
Number of ordered waters	195	185	195 (51**)	185 (42**)
Average B values	12.3	13.1	See Table 2	See Table 2
RMSD bond lengths (Å)	0.016	0.016	0.016	0.016
RMSD bond angles (°)	2.29	2.40	2.29	2.40
Ramachandran distribution				
Most favored (%)	88.7	91.5	89.9	89.9
Allowed (%)	11.3	8.5	10.1	10.1
PDB accession code	1OT9	1OT6	1OT9	1OT6

*RMSD, root mean square deviation; WT, wild type.
†The ground state data is also discussed in an accompanying reference (14).
‡Value in parentheses refer to the last shell.
§$R_{merge} = \Sigma_{hkl}\Sigma_i |I_i - \langle I \rangle|/\Sigma_{hkl}\Sigma_i I_i$, for all data.
‖$R_{cryst} = \Sigma_{hkl} |Fo - Fc|/\Sigma_{hkl}|Fo|$, includes all data.
¶Difference R_{cryst} for cryotrap data $= \Sigma_{hkl} |(Fo^{cryotrap} - Fo^{dark}) - (Fc^{cryotrap} - Fc^{dark})|/\Sigma_{hkl} |Fo^{cryotrap} - Fo^{dark}|$, includes all data.
#R_{free} uses 5% of the data for the test set.
**The number of water molecules that changed from the ground state location.

small, 6.1% for the wild type and 4.1% for the mutant ($R_{diff} = \Sigma_{hkl} |Fo^{cryotrap} - Fo^{dark}|/\Sigma_{hkl}|Fo^{dark}|$). Difference refinement produces a more accurate structure of the cryotrapped state because it refines only the minor structural changes produced by illumination and is not biased by any residual electron density arising from inaccurate modeling of the ground (dark) state.

Refinement of the cryotrapped state. An identical procedure was followed for both the wild type and the E46Q mutant. We determined that there were multiple conformations present in both cryotrapped data sets through close examination of difference and residual electron density maps (see Results). It was necessary to conduct a cautious and deliberate refinement process because the results could easily be perturbed by the spatially overlapping electron density. The first stage was to identify the number of structural species present and estimate their relative occupancies. We assumed that the ground state component of the cryotrapped state has the same conformation as the molecules in the crystal before photoactivation. The ground state structure was independently refined against data collected in the dark (14), and its structure was subsequently kept fixed during refinement of the cryotrapped state. The occupancy of the ground state component was estimated by adjusting its value until no ground state electron density remained in $Fo^{cryotrap} - Fc^{dark}$ residual electron density maps. Such maps revealed strong, well-ordered electron density associated with multiple thioester sulfur positions. These sulfur positions were used as the starting point for identification of the number of photoactivated species and estimation of their relative occupancy.

Once the number of photoactivated species was identified, models of the photoactivated chromophores were built into the appropriate electron density. That is, the atomic model associated with the thioester sulfur with the highest occupancy was fit into the strongest electron density. Although multiple structures were required for the chromophore and Cys69, the rest of the protein could be satisfactorily refined as two homogeneous species: one associated with the fixed ground state structure and the other with the two *cis* species (see Results).

Bond angle and distance restraints were necessary for refinement of the photoactivated chromophore models, but accurate values are unknown because the chromophore might adopt strained, high-energy conformations. We generated stereochemical restraints from the ground state model by making several assumptions about the structures of the various photoactivated species. We assumed initially that the chromophore phenolate ring, the O1′ oxygen and C3 carbon (Fig. 4a) remain planar and retain the bond distances and angles of the ground state; and that the carbonyl group (S, C1, C2 and O1 in Fig. 4a) in the chromophore tail remains planar. We restrained the bond distances and angles in the chromophore tail to the values of the refined ground state model. Because these assumptions may not strictly hold for all chromophore models, the restraints were gradually relaxed by increasing their standard deviations. The planarity restraint for the carbonyl group was fully removed because this moiety could potentially become protonated and pucker.

The chromophore structures were initially refined with their occupancies, B values and thioester sulfur positions fixed. After convergence, their occupancies and that of the ground state were added as additional parameters during refinement of atomic positions. Distance, angle and planarity restraints in the chromophore tail were gradually relaxed, and finally the isotropic B values were refined.

We assessed the progress of the refinement by monitoring the value of R_{free}; the same set of reflections was used for the cryotrapped and dark states. Because the absolute value of R_{free} is of limited usefulness in difference refinement, progress was also critically assessed using residual electron density maps. Refinement was considered to be progressing well if significant electron density features in the residual maps diminished in magnitude. We judged that the refinement had converged when no significant features remained in the residual maps.

RESULTS

Cryotrapped states at 110 K

The cryotrapped state was created by continuous illumination of space group $P6_3$ crystals at 110 K. Ground and cryotrapped data were collected on both wild-type PYP and the E46Q mutant to very high resolution, between 0.95 and 1.05Å, with high redundancy and excellent data quality as judged by the values of I/σI and R_{merge} (Table 1). We collected complete data sets on both proteins,

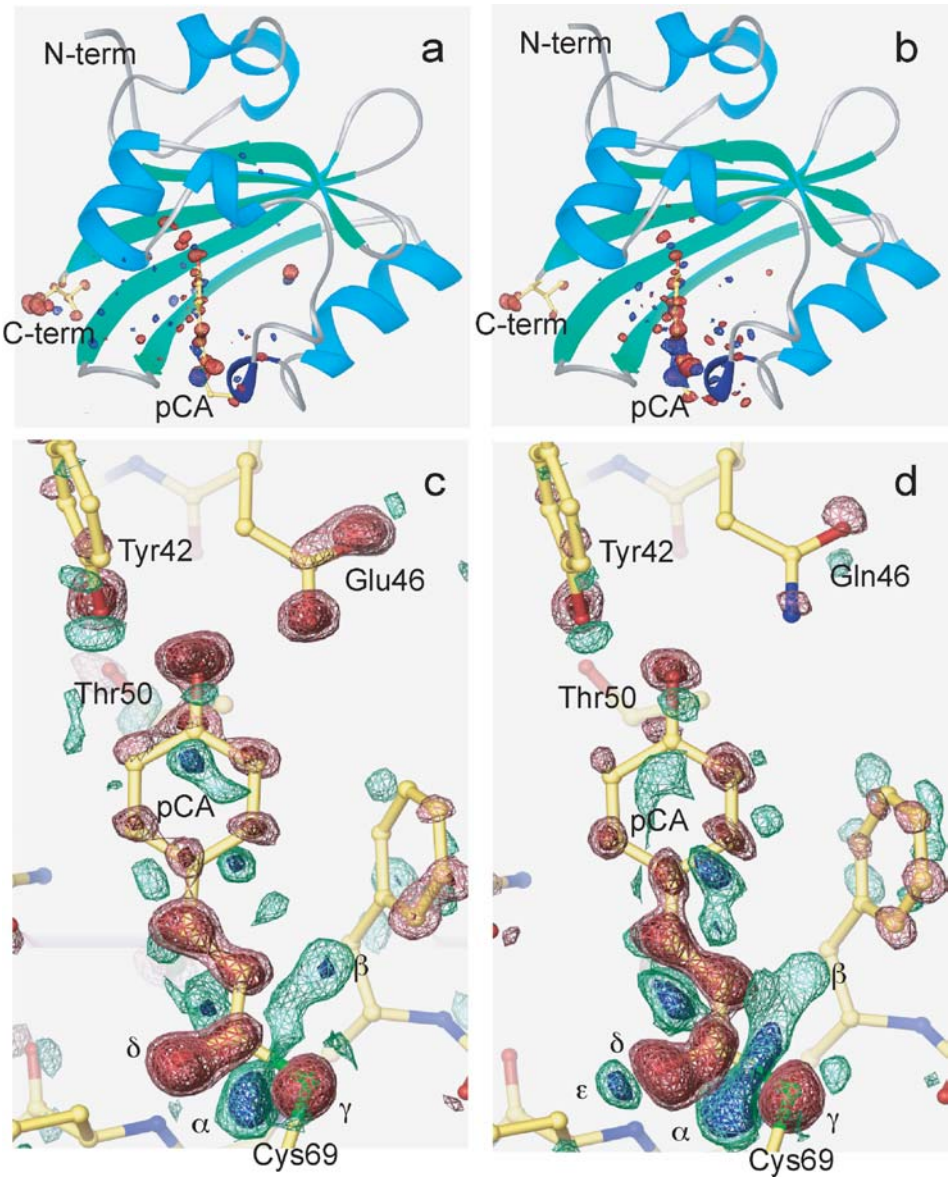

Figure 1. Difference electron density maps showing the difference between the cryotrapped and dark states ($Fo^{cryotrap} - Fo^{dark}$), superimposed on the ground state model. Red and blue contours denote negative and positive difference electron densities, respectively. The entire molecule contoured at $\pm 5\sigma$ for (a) wild type and (b) the E46Q mutant. The chromophore-binding pocket contoured at $\pm 4\sigma$ and $\pm 8\sigma$ for (c) wild type and (d) the E46Q mutant.

both in the dark and after illumination, to establish the cryotrapped state. Difference electron density maps between the two data sets collected on the same crystal observe the structural changes induced in the cryotrapped state. Our results successfully reproduce those on wild-type PYP (10): the $Fo^{cryotrap} - Fo^{dark}$ difference electron density features in our wild-type cryotrapped state at 110 K are nearly identical to those at 149 K (compare our Fig. 1 with fig. 3c of Genick *et al*. 1998). This similarity in results is expected because we deliberately used comparable experimental conditions.

The difference electron density between the cryotrapped and ground state is restricted to the chromophore-binding pocket in both wild-type PYP and its isosteric E46Q mutant (Fig. 1a,b). There are only minor differences between the cryotrapped states formed in wild-type PYP and the mutant; most of the difference electron density features are identical in location, but certain peaks have slightly different magnitudes (compare Fig. 1c,d). The major distinctions include a positive peak ($>6\sigma$) present only in the E46Q difference map adjacent to the ground state carbonyl oxygen (feature ''ε'' in Fig. 1d) and negative electron density on the Glu46 carboxylate oxygens in wild-type PYP that is nearly absent on the mutant Gln46 side chain.

The carboxylic acid moieties adjacent to the chromophore in both wild-type PYP and the E46Q mutant have associated negative electron density but lack any corresponding positive electron density (Fig. 1a,b). Negative difference electron density is present on the Glu46 carboxylate oxygens in wild-type PYP, and the α-carboxylate oxygens and their surrounding hydration shells in both wild type and the E46Q mutant. Although the C-terminus is distant from the chromophore, crystal-packing interactions place the chromophore-binding pocket of one molecule next to the C-terminal α-carboxylate of its neighbor. The absence of associated positive density suggests that the negative density arises from an accelerated rate of X-ray radiation damage–induced decarboxylation near the chromophore (17,18) due to local heating from energy released by the absorbed photons (19). No other carboxylates in either crystal exhibit these negative features.

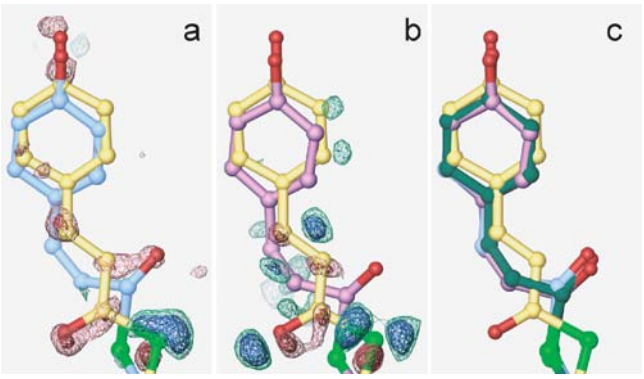

Figure 2. Residual electron density maps after refinement of one photoactivated chromophore model and the ground state model into the cryotrapped state. Electron density is contoured at ±4σ and ±8σ, red negative and blue positive. Residual electron density is shown superimposed over the ground state model, yellow, and single photoactivated model for (a) wild type, light blue and (b) E46Q mutant, purple. (c) Overlay of the wild-type ground state model, yellow, with the single photoactivated models from wild type, light blue, E46Q mutant, purple, and published wild type, green (PDB entry 3PYP) (10).

Structural heterogeneity of the chromophore in the cryotrapped electron density

The ground state of both wild-type PYP and its E46Q mutant could be accurately refined using single atomic models for the chromophore (14), in which Fo–Fc residual maps display no significant features on or around the chromophore (data not shown). We, therefore, initially attempted to refine a single atomic model for the chromophore into the photoactivated component of the wild-type PYP and the E46Q mutant cryotrapped states. As would be expected considering the close similarities in difference electron densities, the refined model in both species was nearly identical to that of the photoactivated chromophore model previously refined into the cryotrapped state produced in wild-type PYP at 149 K (Protein Data Bank [PDB] entry 3PYP) (10). However, even after extensive refinement, highly significant, residual electron density peaks (>8σ) remain in both Fo–Fc residual electron density maps (Fig. 2a,b). The location of this residual electron density is such that no adjustment of a single structure could possibly account for all electron density. That is, no single atomic model fits the data, for either wild-type PYP or its E46Q mutant.

We closely reinspected the difference electron density maps after it became apparent that the cryotrapped state is structurally complex. Although the tail of the chromophore is clearly displaced from its ground state location, the positive difference electron density associated with new tail position(s) is not directly interpretable (Fig. 1c,d). The magnitude of negative electron density on the ground state sulfur location (feature ''γ'' in Fig. 1) is approximately the same as that on the ground state carbonyl oxygen location (feature ''δ'' in Fig. 1), which is unexpected considering that sulfur has twice the number of electrons as oxygen.

Although difference electron density maps are extremely sensitive to small changes in electron density, they can be difficult to interpret. We wish to directly observe the electron density associated with the photoactivated component of the cryotrapped state, but the predominant ground state component masks this electron density in traditional 2Fo–Fc electron density maps. Even with continuous illumination on the crystal, the majority of molecules in the cryotrapped state are found in the ground state conformation (76% in wild type and 65% in the E46Q mutant). To isolate the electron density of the photoactivated component of the cryotrapped state, we subtracted the electron density of the ground state component. We used the assumption that the conformation of the ground state component of the cryotrapped state is identical to that determined for the ground state in the same crystal before illumination. The occupancy of this ground state component was initially estimated by visual inspection of residual maps but later refined along with the conformation and occupancy of the photoactivated models.

The residual maps produced after subtraction of the ground state component of the cryotrapped state show three discrete peaks associated with the thioester sulfur, two of which are close to the ground state position (features ''χ,'' ''ψ'' and ''ω'' in Fig. 3). The positions of these peaks are nearly identical in the wild type and E46Q cryotrapped states, but their magnitudes differ. The presence of the three discrete thioester sulfur locations (in addition to that for the ground state) shows that the photoactivated component contains at least three species. We emphasize that this is a qualitative result, derivable by inspection of an initial residual map, and independent of any stereochemical assumptions or refinement.

Refinement of the heterogeneous mixture of photoactivated species

A chromophore model was independently built and refined for each of the three thioester sulfur positions in both wild type and the E46Q mutant. These three chromophore models were able to account for all electron density in the photoactivated component of the cryotrapped state (Fig. 3d,h), while using only limited isotropic B value refinement and adhering to general stereochemical restraints derived from the ground state model (see Methods). The wild type and the E46Q mutant structures refined into nearly identical coordinates but with different occupancies (Fig. 4). One photoactivated model has the chromophore in an alternate, *trans* conformation and two have *cis* conformations.

The alternate *trans* species has the C2 and C3 carbons of the chromophore tail displaced relative to the ground state (Fig. 4b), but the new position for the thioester sulfur (feature χ in Fig. 3) is only slightly shifted from that in the ground state. This species is present at 14% occupancy in the E46Q mutant and forms the predominant photoactivated species. The significant positive feature that is apparent only in the E46Q electron difference map (feature ε in Fig. 1d) arises from the new location of the carbonyl oxygen in this species. Although the structurally identical *trans* species is also found in wild type, it is present at only 6% occupancy and was not readily apparent until the two other species were modeled at appropriate occupancies.

We refer to the two photoactivated models with *cis* chromophore conformations as *cis*–planar (Fig. 4d) and *cis*–wobble (Fig. 4c). The chromophore conformations are very similar, with the most notable difference being the position of the thioester sulfur. The sulfur position in the *cis*–planar species remains near that of the ground state, whereas in the *cis*–wobble species it has shifted via rotation about the Cβ–S and S–C1 bonds (Fig. 4). In the *cis*–planar species, the carbonyl group in the chromophore tail remains coplanar with the phenolate group, a conformation that is ideal for π orbital overlap and extended electronic conjugation (Table 2). However, the carbonyl O1 makes close contact with the C6′ carbon: 2.8Å in wild type and 2.7Å in the E46Q mutant. Although carbon atoms are capable of serving as hydrogen bond donors

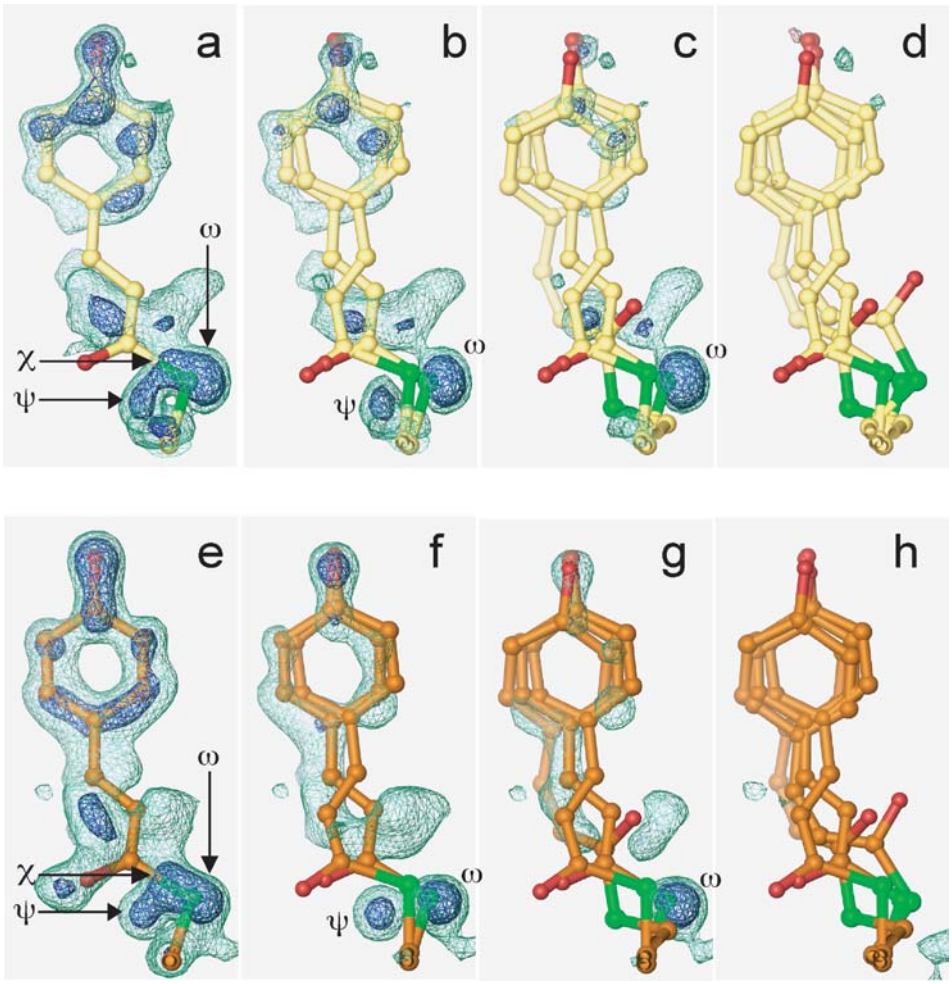

Figure 3. Residual electron density maps after progressive addition of atomic models. Yellow models, wild type; orange, E46Q mutant. Both are superimposed on residual electron density contoured at $\pm 1\sigma$ and $\pm 3\sigma$, blue positive and red negative. (a) Wild-type ground state at 76% occupancy. (b) As in (a) with addition of alternate *trans* at 6% occupancy. (c) As in (b) with addition of *cis*–wobble at 7% occupancy. (d) As in (c) with addition of *cis*–planar at 11% occupancy. (e) E46Q mutant ground state at 65% occupancy. (f) As in (e) with addition of alternate *trans* at 14% occupancy. (g) As in (f) with addition of *cis*–wobble at 8% occupancy. (h) As in (g) with addition of *cis*–planar at 13% occupancy.

(20,21), the distance between the chromophore ring carbon and the carbonyl oxygen is still shorter than expected for a weak hydrogen bond. This close contact is therefore likely to be a destabilizing factor, which is balanced against the energetic strain from distorting bond angles or loss of extended conjugation.

The new position of the thioester sulfur in the *cis*–wobble species (feature ψ in Fig. 3) creates the largest positive peak in the difference electron density maps (feature ''α'' in Fig. 1) even though the occupancy is only 7% in wild type and 8% in the E46Q mutant. The large magnitude of this peak is a result of displacing the electron-rich sulfur to a new position that is unoccupied in the ground state. The *cis*–wobble species can readily convert into the *cis*–planar species by motion of the thioester sulfur. Moving the sulfur rotates the chromophore and creates a steric clash with the side chain of Phe96, which necessitates a twisting of the chromophore in its binding pocket. The carbonyl moiety in the *cis*–wobble species is displaced out of the plane of the chromophore. This species has therefore lost extended electronic conjugation compared with the *cis*–planar species and has also lost the steric clash between O1′ and C6′. The phenolate ring of the chromophore is only slightly displaced in all photoactivated species; therefore, the hydrogen bond network to its phenolate oxygen is maintained (Table 2).

The low occupancy of several photoactivated species made it unfeasible to refine separate atomic positions for all protein residues in each species. We, therefore, refined two structures for the protein residues: one associated with the alternate *trans* species and ground state, and the other with the two *cis* species. The conformation of the alternate *trans* chromophore is very similar to that in the ground state, and in particular, both species have the chromophore phenolate oxygen in nearly identical positions. This strategy produced chemically plausible results for the protein structures surrounding the chromophore, with reasonable hydrogen bond lengths (Table 2).

Coordinates for all protein structures have been deposited in the PDB (Table 1).

DISCUSSION

Interpretation of structural heterogeneity

Although our experimental results for the cryotrapped state of wild-type PYP at 110 K are nearly identical to those obtained previously at 149 K (10), our interpretation is significantly different. It is apparent from close inspection of the difference electron density maps that the photoactivated component of the cryotrapped state is complex and cannot be modeled with a single atomic structure. Traditional refinement with a single atomic model produces an extremely strained structure that still does not account satisfactorily for all electron density because residual features remain with a peak height as large as $\pm 8\sigma$ (Fig. 2). This strained structure was described as a transition state–like intermediate in the

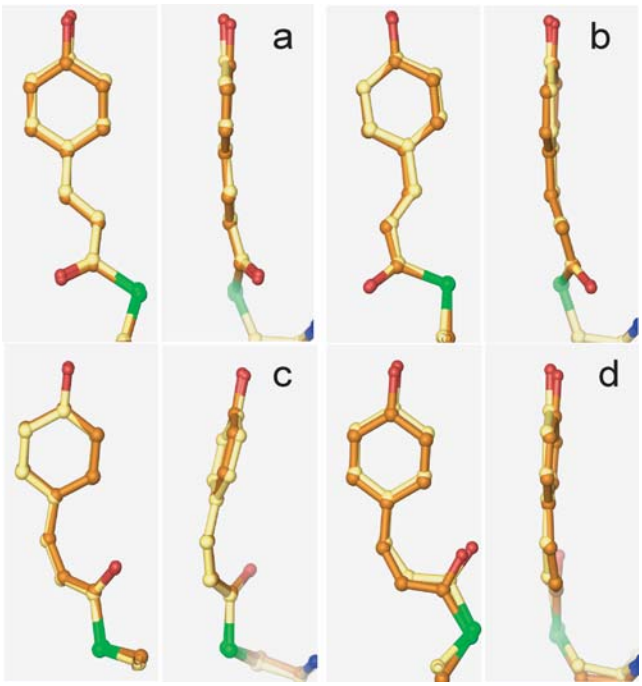

Figure 4. Front and side views of the four chromophore models refined into the cryotrapped state. Yellow models, wild type; orange models, E46Q mutant. (a) Ground state. (b) Alternate *trans*. (c) *cis*–wobble. (d) *cis*–planar.

previous experiment because bond angles in the carbonyl group of the chromophore tail are significantly perturbed from normal (11). It now appears that this apparent intermediate is a consequence of the refinement procedure and not an authentic, homogeneous structure populated in the crystal.

The refinement and interpretation of even the highest resolution data must be performed with care when working with heterogeneous populations. The low occupancy of each species and the spatially overlapped electron density made refinement difficult. It could be attacked successfully only because high-quality data to very high resolution were available on independent crystals of wild type and the E46Q mutant. Given the discrete electron density peaks associated with the thioester sulfur in the residual maps, it was impossible to adequately account for all electron density with less than four structures (three for the photoactivated component plus one for the ground component). Because the electron density of all species largely overlapped in space, it was essential to identify and model each to permit accurate refinement of them all. Although the initial intent of this experiment was to examine differences between the cryotrapped states of wild type and the E46Q mutant, the fact that their cryotrapped states were so similar was the key to unraveling the heterogeneous mixture. Although we deliberately did not restrain the wild type and E46Q models to be the same, refinement against independent data sets produced nearly identical structures (Fig. 4). This similarity is especially significant because the proportional occupancies of the relative species differ in the two data sets. We find that a mixture of nearly identical structures at different occupancies fully accounts for all electron density in both the wild-type PYP and E46Q mutant cryotrapped states.

We considered the possibility that incorrect modeling of the ground state may have perturbed our analysis of the cryotrapped state; any ground state electron density not represented by the model would propagate into the residual electron density maps representing the photoactivated component of the cryotrapped state. Both the wild-type and ground state models were refined with anisotropic B factors and fully account for all electron density in the ground state data sets (data not shown), but the ground state component of the cryotrapped state may be slightly shifted relative to the ground state model. Although such a shifted conformation could potentially produce a thioester sulfur peak in residual electron density maps, it would also present additional electron density closely overlaying the remainder of the ground state model of the chromophore tail. No such electron density was present, and we conclude that the ground state has been accurately modeled.

Chromophore isomerization in the early stages of the photocycle

Our cryotrapping experiment has identified chromophore conformations that are accessible through isomerization within a relatively rigid chromophore-binding pocket. These photoactivated species are potentially related to the early, very short-lived intermediates in the room temperature photocycle. The fundamental assumption necessary to connect these species observed in the cryotrapped state to the earliest room temperature intermediates is that at

Table 2. Chromophore geometries and hydrogen bond lengths. Hydrogen bond lengths (Å) are given between the groups noted. Planarity angle denotes the angle between the plane of the chromophore phenolate ring and plane of the carbonyl group. The far right column gives the average B value of chromophore atoms*

	Hydrogen bond lengths (Å)					
	E/Q46 to	Y42 to				
Species	pCA phenolate oxygen		T50 to Y42	C69 N to pCA O1	Planarity angle (°)	Chromophore (B value)
E46Q ground state	2.88 ± 0.02	2.48 ± 0.02	2.78 ± 0.02	2.74 ± 0.02	29	7.4
WT ground state	2.59 ± 0.02	2.50 ± 0.02	2.85 ± 0.02	2.75 ± 0.02	26	6.2
E46Q alternate *trans*	2.8	2.5	2.8	2.5	34	7.9
WT alternate *trans*	2.7	2.5	2.8	2.5	27	6.8
E46Q *cis*–wobble	3.1	2.6	2.8	NA	38	8.9
WT *cis*–wobble	3.1	2.8	2.8	NA	45	7.0
E46Q *cis*–planar	3.0	2.7	2.8	NA	3	7.6
WT *cis*–planar	2.6	2.6	2.8	NA	7	6.7

*NA, not applicable; pCA, *para*-coumaric acid; WT, wild type.

room temperature, atoms in the photoactivated chromophore move rapidly with respect to those in neighboring protein residues. That is, it takes a relatively long time for the surrounding protein to undergo a concerted structural rearrangement to accommodate the highly vibrationally and electronically activated chromophore. This situation can be simulated over much longer timescales by examining the protein at cryogenic temperatures.

Although we can directly observe the photoactivated chromophore conformations at low temperature, these species may not be identical in all respects to species formed early in the room temperature photocycle. We continuously illuminated the crystal throughout data collection to accumulate a significant proportion of molecules in the photoactive state. Prolonged illumination could generate species arising from multiphoton absorption, a process that would be extremely rare during photoactivation under physiological conditions. Indeed, we were surprised when our analysis of the photoactivated component revealed an alternate *trans* conformation of the chromophore. This conformation may arise from absorption of a second photon by a *cis* species.

Although this alternate *trans* conformation is likely to be an artifact of the experiment, the structures of the two *cis* species give insight into the mechanism of chromophore isomerization. The simplest mode of chromophore isomerization in PYP would require a hula-twist motion about the C3 carbon (22), which produces a *cis* chromophore in which the carbonyl is retained on the ground state side of the tail of the chromophore. A *cis* chromophore in this conformation would be energetically unfavorable because of steric hindrance, and thus the *cis* chromophore would promptly relax into the relatively stable, *cis*–planar conformation by flipping the carbonyl group to the opposite side of the tail. The carbonyl group would then revert to the ground state side in the subsequent progression to the pR intermediate (9,23). The relatively disordered *cis*–wobble species suggests a mechanism by which the flips can be achieved. The alternative thioester sulfur position in the *cis*–wobble species is formed when both the sulfur and the carbonyl group move out of the chromophore plane. Model building shows that the carbonyl group in the *cis*–wobble orientation can revert to the ground state side of the chromophore tail by rotation of the entire carbonyl group, without steric hindrance from neighboring atoms. The carbonyl moiety can therefore be flipped by first, shifting the thioester sulfur by simultaneous rotation about the Cβ–S and S–C1 bonds, and second, complete rotation of the entire carbonyl group to reestablish the original thioester location.

All the photoactivated species in the cryotrapped state are the same in wild type and the E46Q mutant, which implies that the chromophore isomerization processes in the early stages of the room temperature photocycle are identical. The faster overall photocycle in the E46Q mutant is therefore a result of subtle electronic and structural differences arising from its longer, weakened hydrogen bond from Gln46 to the chromophore phenolate oxygen and consequently looser chromophore-binding pocket (14).

CONCLUSIONS

The electron density produced in PYP under continuous illumination at 110 K cannot be accurately modeled by a single, highly strained structure. Rather, it arises from a mixture of species, each one of which has reasonable stereochemistry. Although refinement was challenging because of spatially overlapping electron density and low occupancy, the validity of the three refined structures is bolstered by the nearly identical structures produced by independent refinement of wild-type PYP and the E46Q mutant. This study is based on the highly detailed information that can be obtained from carefully collected data at very high resolution. However, it also emphasizes the potential problems that can arise from applying traditional refinement practices to heterogeneous mixtures. Because even the best manipulation of conditions can produce elements of heterogeneity, results from trapping experiments must be treated with caution.

Acknowledgements—Thanks to the staff at BioCARS and fellow graduate students Sean Crosson and Jason Key for help with data collection. Thanks also to Carl Correll, Wouter Hoff and Anthony Kossiakoff for their critical input. This work was supported by National Institutes of Health Grant GM36452 (K.M.), and the BioCARS facility at the Advanced Photon Source is supported by National Institutes of Health Grant RR07707 (K.M.).

REFERENCES

1. Meyer, T. E. (1985) Isolation and characterization of soluble cytochromes, ferredoxins and other chromophoric proteins from the halophilic phototrophic bacterium *Ectothiorhodospira-Halophila*. *Biochim. Biophys. Acta* **806**, 175–183.
2. Cusanovich, M. A. and T. E. Meyer (2003) Photoactive yellow protein: a prototypic PAS domain sensory protein and development of a common signaling mechanism. *Biochemistry* **42**, 965–970.
3. Hellingwerf, K. J., J. Hendriks and T. Gensch (2003) Photoactive yellow protein, a new type of photoreceptor protein: will this ''yellow lab'' bring us where we want to go? *J. Phys. Chem. A* **107**, 1082–1094.
4. Van der Horst, M. A. and K. J. Hellingwerf (2004) Photoreceptor proteins, ''star actors of modern times'': a review of the functional dynamics in the structure of representative members of six different photoreceptor families. *Acc. Chem. Res.* **37**, 13–20.
5. Ujj, L., S. Devanathan, T. E. Meyer, M. A. Cusanovich, G. Tollin and G. H. Atkinson (1998) New photocycle intermediates in the photoactive yellow protein from *Ectothiorhodospira halophila*: picosecond transient absorption spectroscopy. *Biophys. J.* **75**, 406–412.
6. Hoff, W. D., S. L. S. Kwa, R. van Grondelle and K. J. Hellingwerf (1992) Low-temperature absorbency and fluorescence spectroscopy of the photoactive yellow protein from *Ectothiorhodospira-halophila*. *Photochem. Photobiol.* **56**, 529–539.
7. Imamoto, Y., M. Kataoka and F. Tokunaga (1996) Photoreaction cycle of photoactive yellow protein from *Ectothiorhodospira halophila* studied by low-temperature spectroscopy. *Biochemistry* **35**, 14047–14053.
8. Imamoto, Y., M. Kataoka, F. Tokunaga, T. Asahi and H. Masuhara (2001) Primary photoreaction of photoactive yellow protein studied by subpicosecond-nanosecond spectroscopy. *Biochemistry* **40**, 6047–6052.
9. Ren, Z., B. Perman, V. Srajer, T. Y. Teng, C. Pradervand, D. Bourgeois, F. Schotte, T. Ursby, R. Kort, M. Wulff and K. Moffat (2001) A molecular movie at 1.8 Å resolution displays the photocycle of photoactive yellow protein, a eubacterial blue-light receptor, from nanoseconds to seconds. *Biochemistry* **40**, 13788–13801.
10. Genick, U. K., S. M. Soltis, P. Kuhn, I. L. Canestrelli and E. D. Getzoff (1998) Structure at 0.85 Å resolution of an early protein photocycle intermediate. *Nature* **392**, 206–209.
11. Essen, L. O. and D. Oesterhelt (1998) A cold break for photoreceptors. *Nature* **392**, 131–133.
12. Genick, U. K., S. Devanathan, T. E. Meyer, I. L. Canestrelli, E. Williams, M. A. Cusanovich, G. Tollin and E. D. Getzoff (1997) Active site mutants implicate key residues for control of color and light cycle kinetics of photoactive yellow protein. *Biochemistry* **36**, 8–14.
13. Mihara, K., O. Hisatomi, Y. Imamoto, M. Kataoka and F. Tokunaga (1997) Functional expression and site-directed mutagenesis of photoactive yellow protein. *J. Biochem. (Tokyo)* **121**, 876–880.
14. Anderson, S., S. Crosson and K. Moffat (2004) Short hydrogen bonds in photoactive yellow protein. *Acta Crystallogr.* **D60,**1008–1016.
15. Otwinowski, Z. and W. Minor (1997) Processing of X-ray diffraction data collected in oscillation mode. *Methods Enzymol.* **276**, 307–326.
16. Terwilliger, T. C. and J. Berendzen (1995) Difference refinement—obtaining differences between 2 related structures. *Acta Crystallogr. D.* **51**, 609–618.

17. Weik, M., R. B. G. Ravelli, G. Kryger, S. McSweeney, M. L. Raves, M. Harel, P. Gros, I. Silman, J. Kroon and J. L. Sussman (2000) Specific chemical and structural damage to proteins produced by synchrotron radiation. *Proc. Natl. Acad. Sci. USA* **97**, 623–628.
18. Burmeister, W. P. (2000) Structural changes in a cryo-cooled protein crystal owing to radiation damage. *Acta Crystallogr. D.* **56**, 328–341.
19. van Brederode, M. E., T. Gensch, W. D. Hoff, K. J. Hellingwerf and S. E. Braslavsky (1995) Photoinduced volume change and energy-storage associated with the early transformations of the photoactive yellow protein from *Ectothiorhodospira-Halophila*. *Biophys. J.* **68**, 1101–1109.
20. Steiner, T. and G. R. Desiraju (1998) Distinction between the weak hydrogen bond and the van der Waals interaction. *Chem. Commun.* **8**, 891–892.
21. Steiner, T. (2002) The hydrogen bond in the solid state. *Angew. Chem. Int. Edit.* **41**, 48–76.
22. Liu, R. S. H. and G. S. Hammond (2001) Examples of hula-twist in photochemical *cis-trans* isomerization. *Chem. Eur. J.* **7**, 4536–4544.
23. Anderson, S., V. Srajer, R. Pahl, S. Rajagopal, F. Schotte, P. Anfinrud, M. Wulff and K. Moffat (2004) Chromophore conformation and the evolution of tertiary structural change in photoactive yellow protein. *Structure* **12**, 1039–1045.